Solvothermal Synthesis and Crystal Structures of Alkali Molybdates

by **Alexej Michailovski**[a]), **Johannes B. Willems**[a]), **Norbert Stock**[b]), and **Greta R. Patzke***[a])

[a]) Laboratory of Inorganic Chemistry, ETH Hönggerberg, Wolfgang-Pauli-Strasse 10, CH-8093 Zürich (phone: +41-44-6326743; fax: +41-44-6321149; e-mail: patzke@inorg.chem.ethz.ch)

[b]) Institute of Inorganic Chemistry, Christian-Albrechts-Universität, Otto-Hahn-Platz 6/7, D-24098 Kiel

Within the frame of systematic morphological studies concerning the solvothermal formation of nanoscale and microscale molybdenum oxides from the interaction of a molybdenum-based precursor such as $MoO_3 \cdot 2\,H_2O$ with ionic additives such as alkali and earth alkali halides, we studied – with the aim to elaborate preparative guidelines – the influence of the precursor structure and the alkali halide upon the crystal structure of the emerging alkali polymolybdates in terms of solvothermal fields and high-throughput solvothermal techniques. The discussion of the resulting crystal structures revealed a structure-directing potential of the alkali cations that was explored for the synthesis of new mixed alkali polymolybdates.

1. Introduction. – Over the past decades, solvothermal reactions have become a powerful tool in inorganic and materials chemistry [1]. They provide straightforward synthetic procedures and the option of morphology control from the millimeter to the nanometer scale [2–7]. This renders them especially useful for nanotechnological applications [8]. Although solvothermal methods are widely used, their theoretical background is difficult to explore [9][10], and considerable optimization work may be required to address a synthetic target.

The present systematic study results from our previous work on the solvothermal growth of MoO_3 nanorods [11–13]. The catalytic activity [14–17] and the sensing properties [18] of MoO_3 have attracted considerable interest. We have, therefore, established a one-step straightforward solvothermal routine that provides a quick and quantitative access to MoO_3 fibers with high aspect ratios. The influence of ionic additives, *e.g.*, alkali halides, on the solvothermal process was investigated [11], and it was found that halides of the heavier alkali ions (K^+ to Rb^+) favor the formation of crystalline polymolybdates(VI). The latter are known for their rich and fascinating structural chemistry [19–22]. As a consequence, the development of precise synthetic pathways to a desired modification often remains a preparative challenge [23][24]. Predictive inorganic synthesis is an intriguing topic so that a controlled synthetic approach towards inorganic materials often requires profound parameter studies and experimental effort.

In this context, our convenient and flexible solvothermal protocol has now been employed for tracking down structure–synthesis relationships among caesium and rubidium polymolybdates(VI): *1*) First, the influence of selected reaction parameters (especially the structure of the Mo-based precursor and the reaction temperature) on the crystal structure of the products was explored in terms of systematic solvothermal

fields. *2*) The emerging crystal structures are discussed with emphasis on the role of the larger alkali cations (Rb^+ to Cs^+). *3*) Finally, the structure chemistry of novel mixed alkali fluoromolybdates was explored with high-throughput solvothermal methods [25–29].

2. Experimental. – In a standard solvothermal experiment, precursor material containing Mo (1 mmol) (*e.g.*, $MoO_3 \cdot 2\,H_2O$ (180 mg), synthesized from sodium molybdate and $HClO_4$ [30]), H_2O (2 ml), and the appropriate alkali iodide or fluoride (2 mmol) were added to a *Teflon*-lined stainless-steel autoclave with a capacity of 23 ml. The autoclave was then sealed, heated for 2 d at 100–220°, and subsequently cooled to r.t. All experiments are summarized in *Figs. 1* and *2*. The resulting precipitate was collected by filtration, washed with distilled H_2O, EtOH, and Et_2O or acetone, and dried in air. X-Ray powder diffraction analyses were conducted with a *Stoe-STADI-P2* diffractometer in transmission mode (flat sample holders, Ge-monochromated Cu$K_{\alpha 1}$ radiation) equipped with a position-sensitive detector (resolution *ca.* 0.01° in 2θ). A *CamScan-CS-44* electron microscope with an *EDAX-Phoenix* energy-dispersive X-ray spectrometer (*EDXS*) was employed for approximate elemental analyses. F-Contents were determined by ion chromatography with a *Metrohm 761 Compact IC*. X-Ray diffraction data for $Cs_2Mo_3O_{10} \cdot H_2O$ were collected on a *Stoe-IPDS-I* diffractometer, and data reduction was performed with the program INTEGRATE [31]. All other data were collected with a *Bruker-AXS-SMART-CCD* diffractometer, and the data reduction was performed with the SAINT software [32]. The program XPREP [33] was used for space-group determination. The structures were solved by direct methods (SHELXS-97 [34]) and refined against F^2 with the full-matrix least-squares method (SHELXL-97 [34]). The numerical absorption correction was performed with XPREP [33]. X-RED [35] and X-SHAPE [36] were used for the empirical determination of crystal shape and size. The program SADABS [37] was employed for empirical absorption corrections.

Further details of the crystal-structure investigations may be obtained from the Fachinformationszentrum Karlsruhe, Informationsdienste, Hermann-von-Helmholtz-Platz 1, D-76344 Eggenstein-Leopoldshafen, Germany, on quoting the depository numbers CSD 415308 ($Rb_2Mo_4O_{13}$) and 415310–415313 ($Cs_2Mo_4O_{13}$, $Rb_6Mo_8O_{26}F_2 \cdot 6\,H_2O$, $(NH_4)_{0.13}Cs_{1.87}Mo_3O_{10} \cdot H_2O$, and $(NH_4)_{0.37}Rb_{5.63}Mo_7O_{24} \cdot 4\,H_2O$).

High-throughput solvothermal experiments were performed in a multiclave with 48 miniaturized *Teflon* reactor chambers (diameter 7 mm, depth 13 mm, max. reactant volume 200 µl) [25]. The reaction block was covered with thin *Teflon* sheets and sealed inside the stainless-steel multiclave, followed by heating at 180° for 3 days. After the reaction, the samples were isolated in parallel as an array by centrifugation in a custom-designed centrifuge apparatus and washed in a custom-designed filtration apparatus. The sample array was collected on filter paper in a metal frame that was transferred to a sample holder for automated X-ray analysis. Powder diffractometry was carried out with a newly developed *Stoe*-powder-diffraction instrument for high-throughput measurements in transmission geometry, equipped with an image-plate detector system [25]. The data collection time was 11 min per sample.

3. Solvothermal Fields: Exploring the Preparation of Rubidium and Caesium Molybdates. – 3.1. *Strategy.* Yellow molybdic acid, $MoO_3 \cdot 2\,H_2O$, is a versatile solvothermal precursor that readily gives access to MoO_3 fibers with diameters below 100 nm and lengths extending far into the microscale [13].

The entire alkali halide series (MX, M = Li–Na, X = F–I) were tested for morphology control of the MoO_3 fibers, and only the chlorides and bromides of Li^+ and Na^+ turned out to be suitable additives [11]. Their heavier analogues K^+ to Cs^+ were incorporated into microcrystalline hexagonal molybdates [38][39] instead. In *Fig. 1* (top), a summary of our experiments is given. The heavier alkali iodides and fluorides (MX, M = K–Cs, X = F, I) clearly favor the formation of mm-sized polymolybdate-(VI) crystals. We therefore selected the halides RbX and CsX (X = F, I) for a systematic solvothermal/crystallographic study.

Furthermore, we investigated whether the crystal structure of the products could be addressed by selecting an appropriate precursor material. For this purpose, the

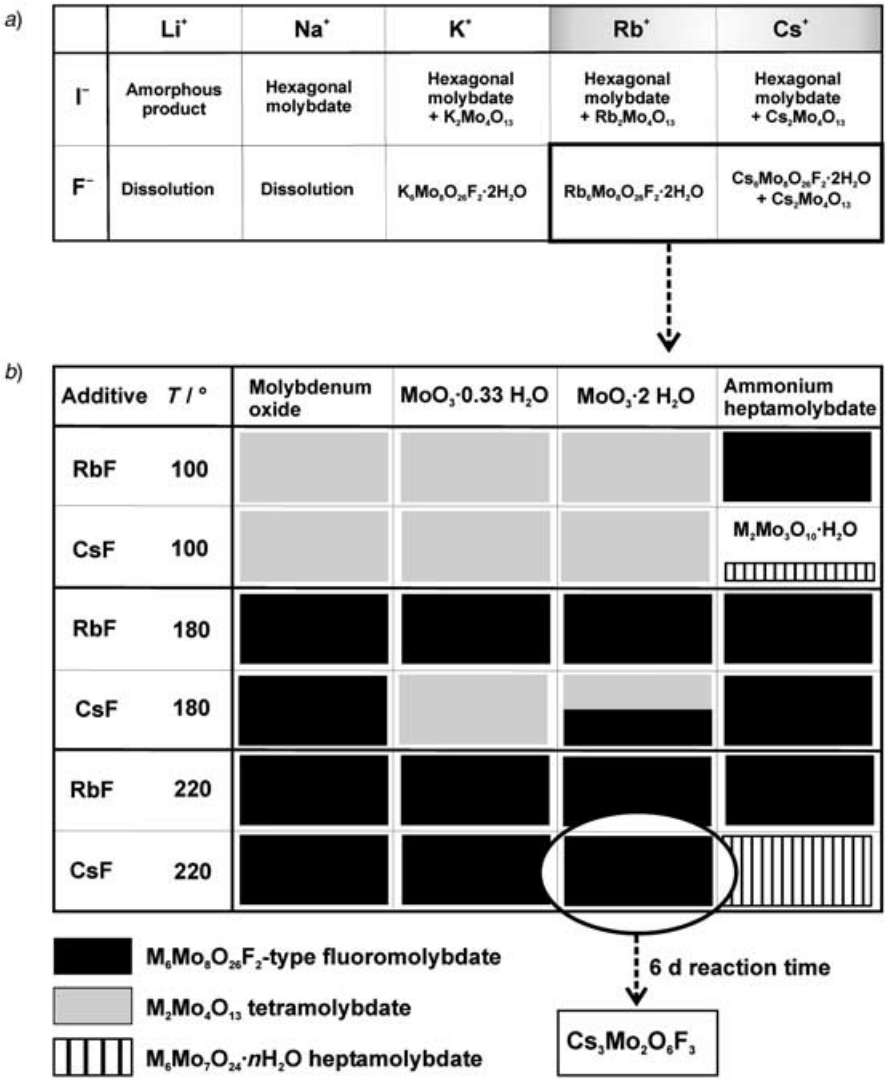

Fig. 1. a) *Results of the alkali halide screening experiments with* $MoO_3 \cdot 2\ H_2O$. b) *Solvothermal field mapping the interaction of molybdenum-based precursor materials with RbF and CsF at 100–220°*. The relative size of the symbols indicating biphasic products is proportional to the ratio of the components.

behavior of the precursor series of the topotactically related MoO_3, $MoO_3 \cdot 0.33\ H_2O$, and $MoO_3 \cdot 2\ H_2O$ towards RbX and CsX (X = F, I) was compared to ammonium heptamolybdate, $(NH_4)_6Mo_7O_{24} \cdot 4\ H_2O$, with a completely different cluster-based structure.

Finally, the influence of the reaction temperature on the structure of the products was investigated. Such temperature/structure guidelines could be useful for generating different molybdate types by a common synthetic protocol.

3.2. *Solvothermal Fields: CsF and RbF.* The interaction of the precursors with CsF and RbF at 100, 180, and 220° was compared under standardized conditions (*Fig. 1*, *cf. Sect. 2*). The structure chemistry of the products is discussed in *Sect. 4*, and further information on the product types is provided in the *Appendix*, *Tables SI-1 – SI-4*.

The solvothermal reaction of the series MoO_3, $MoO_3 \cdot 0.33\ H_2O$, and $MoO_3 \cdot 2\ H_2O$ with CsF or RbF exclusively generates chain-containing $M_2Mo_4O_{13}$ tetramolybdates (M = Rb, Cs; *cf. Table SI-1* and *Sect. 4.2*) and cluster-based $M_6Mo_8O_{26}F_2 \cdot nH_2O$ difluorooctamolybdates (M = Rb, Cs; *cf. Table SI-4* and *Sect. 4.5*). At 100°, phase-pure tetramolybdates are formed. When the temperature is raised to 180°, the formation of difluorooctamolybdates sets in, and they are available in phase-pure form at 220°.

The solvothermal behavior of the reference precursor, ammonium heptamolybdate, is considerably different. RbF exclusively leads to the continuous formation of $Rb_6Mo_8O_{26}F_2 \cdot 6\ H_2O$ over the entire temperature range (100 – 220°), whilst the reaction of ammonium heptamolybdate with CsF varies with the reaction temperature. Lower temperatures (100°) favor the formation of $Cs_2Mo_3O_{10} \cdot H_2O$ (chain structure, *cf. Sect. 4.3*) with $Cs_6Mo_7O_{24} \cdot 7\ H_2O$ as a by-product. At higher temperatures, caesium difluorooctamolybdate (180°) and $Cs_6Mo_7O_{24} \cdot 7\ H_2O$ (220°) are formed.

As will be illustrated by the crystallographic analyses (*cf. Sect. 4.3* and *4.4*), alkali molybdates generated from ammonium heptamolybdate may contain a certain amount of ammonium cations (usually below 7 mol-% of the cations). Therefore, ammonium heptamolybdate might better be replaced by the corresponding alkali heptamolybdates when specific syntheses instead of experimental screening series are to be performed.

The robustness of the synthetic protocol towards alterations of the reaction time was investigated for the $MoO_3 \cdot 2\ H_2O$/CsF subsystem. Both the preparation of $Cs_2Mo_4O_{13}$ (100°) and of caesium difluorooctamolybdate (180°) can be conducted within a time window of 1 – 6 d. At 220°, however, prolonged solvothermal treatments increase the degree of fluorination so that $Cs_3Mo_2O_6F_3$ is formed after 6 d (*Fig. 1* and *Table SI-4*).

Two major synthetic guidelines emerge from the solvothermal field: *i*) *Precursor structure/reactivity:* The common layered structure of the MoO_3-based precursor group MoO_3, $MoO_3 \cdot 0.33\ H_2O$, or $MoO_3 \cdot 2\ H_2O$ gives rise to analogous solvothermal reactivity, whereas the cluster molybdate $(NH_4)_6Mo_7O_{24} \cdot 4\ H_2O$ exhibits a different behavior. *ii*) *Structure/temperature:* Low reaction temperatures (100°) transform the MoO_3-related precursor series into chain molybdates of the $M_2Mo_4O_{13}$ type (M = Rb, Cs). Elevated reaction temperatures (180 – 220°) induce the formation of cluster-based difluorooctamolybdates.

3.3. *Solvothermal Fields: CsI and RbI.* The iodide-based solvothermal field of the MoO_3-related precursor series (*Fig. 2*) is far more complex because the reducing activity of the I-ion favors the formation of blue, microcrystalline hexagonal molybdates. They can be separated mechanically from the colorless macrocrystalline polymolybdates(VI).

$M_2Mo_4O_{13}$ tetramolybdates (*cf. Sect. 4.2*) are the main crystalline product. Furthermore, CsI and RbI provide different preparative pathways: at 180°, *e.g.*, the layered compound $Cs_2Mo_5O_{16}$ is formed from CsI and MoO_3 (or $MoO_3 \cdot 0.33\ H_2O$) [23]. RbI, on the other hand, is capable of generating mm-size crystals of the red molybdenum bronze $Rb_{0.33}MoO_3$ [40] from $MoO_3 \cdot 0.33\ H_2O$ at 220° (*cf. Fig. 2*). This is

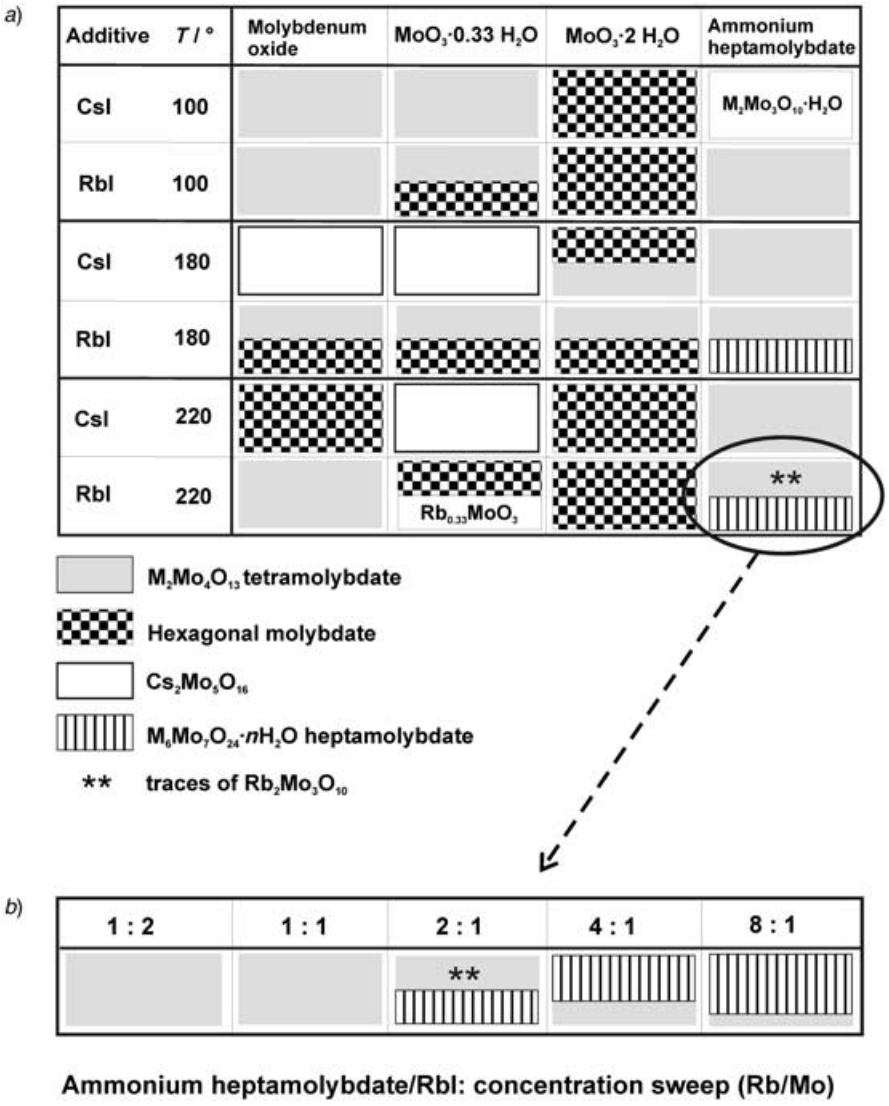

Fig. 2. a) *Solvothermal field displaying the reactivity of the precursor materials* (*cf. Fig. 1*) *towards RbI and CsI at 100–220°*. b) *Optimization of* $Rb_6Mo_7O_{24} \cdot 4\ H_2O$ *synthesis at 220°*

an interesting novel solvothermal approach towards crystalline alkali molybdenum bronzes, because no reductive pretreatment of the educts is required [41].

The use of ammonium heptamolybdate as a precursor prevents the formation of hexagonal molybdates, and $M_2Mo_4O_{13}$ tetramolybdates are formed instead. Like in the fluoride-based field, the reaction of ammonium heptamolybdate with CsI or RbI gives access to tri- and heptamolybdates: $(NH_4)_{0.13}Cs_{1.87}Mo_3O_{10} \cdot H_2O$ is formed at 100° in the presence of CsI (*cf. Fig. 1:* CsF at 100°), and $(NH_4)_{0.37}Rb_{5.63}Mo_7O_{24} \cdot 4\ H_2O$ is generated

at higher temperatures (180–220°) together with $Rb_2Mo_4O_{13}$ (*cf. Fig. 1:* CsF at 220°). As mentioned above, small amounts of ammonium cations may be retained in the products when ammonium heptamolybdate is employed as a precursor. The heptamolybdate/tetramolybdate ratio can be increased when a considerable excess of RbI is applied at 220° (*Fig. 2,b*).

All in all, the two major guidelines derived from the fluoride-based field can be confirmed: *i*) *Precursor structure/reactivity:* Ammonium heptamolybdate withstands the reducing activity of the iodide anion and does not afford hexagonal molybdates, whereas the MoO_3-based-precursor series is readily reduced to hexagonal phases. *ii*) *Structure/temperature:* Elevated reaction temperatures give rise to novel synthetic pathways (formation of highly fluorinated molybdates or red molybdenum bronzes).

In the following, the crystal structures of *t*-$Cs_2Mo_4O_{13}$ and $(NH_4)_{0.13}Cs_{1.87}Mo_3O_{10}\cdot H_2O$ will be discussed first, followed by $(NH_4)_{0.37}Rb_{5.63}Mo_7O_{24}\cdot 4\,H_2O$. Finally, new structural investigations and high-throughput experiments regarding difluorooctamolybdates ($Rb_6Mo_8O_{26}F_2\cdot 6\,H_2O$ and $Cs_6Mo_8O_{26}F_2\cdot nH_2O$) will be presented.

4. Crystal Structures of Rubidium- and Caesium Molybdates. – 4.1. *Scope.* The structure of alkali polymolybdates(VI) strongly depends upon the interaction between the alkali cation and the Mo–O framework: within a given alkali molybdate series, the crystal structures may vary considerably with the size of the alkali cations (*cf. Sect. 4.4* and *4.5* and *Tables SI-1* to *SI-4*). This phenomenon is in the focus of the following structural discussions. As the use of computational methods is beyond the scope of this study, we have described the cationic environments in terms of bond valence sums (BVS) [42] based on the 'largest gap' criterion [43]. The emerging trends inspired us to investigate mixed alkali molybdates (*cf. Sect. 5*).

4.2. *Crystal Structures of $Rb_2Mo_4O_{13}$ and $Cs_2Mo_4O_{13}$.* 4.2.1. *Trends among the Alkali Tetramolybdates.* The effect of the cation size on the polymolybdate(VI) structure is evident for the $M_2Mo_4O_{13}$-type alkali tetramolybdates: both the high-temperature and the low-temperature forms of $Li_2Mo_4O_{13}$ (*H*-[44] and *L*-$Li_2Mo_4O_{13}$ [45]) are derivatives of the V_6O_{13} structure [46], whereas the $[Mo_4O_{13}]^{2-}$ chains in monoclinic $Na_2Mo_4O_{13}\cdot 6\,H_2O$ [47] are linked differently from those in the homotypic *t*-$M_2Mo_4O_{13}$ series (M = K–Cs). Both triclinic $Rb_2Mo_4O_{13}$ [24] and *t*-$K_2Mo_4O_{13}$ [24] (*Table SI-1*) have been prepared by the same solid-state techniques. For the potassium and the ammonium tetramolybdates, orthorhombic modifications have been reported several times [48–50], but no detailed structural information is available for *m*-$K_2Mo_4O_{13}$ [51][52]. $Cs_2Mo_4O_{13}$ is an intriguing substance that illustrates the crucial structure-directing impact of the preparative history: at least seven different modifications have been generated in terms of classical solid-state synthetic techniques, but only one of them has been structurally characterized in detail (*Table SI-2*) [53][54]. Unsuccessful attempts to synthesize *t*-$Cs_2Mo_4O_{13}$ led *Gatehouse* and *Leverett* to the conclusion that '(the tetramolybdate chain) *is disrupted by the much larger caesium ions* (…) *and $Cs_2Mo_4O_{13}$ has a different structure from that of $K_2Mo_4O_{13}$ and $Rb_2Mo_4O_{13}$*' [24]. Our solvothermal fields (*Figs. 1* and *2*) have now brought forward this missing modification.

4.2.2. *The* t-*$M_2Mo_4O_{13}$* (M = K–Cs) *Series.* Parameters for the structure determination of $Rb_2Mo_4O_{13}$ and $Cs_2Mo_4O_{13}$ are summarized in *Tables 1* and *2*. The characteristic $[Mo_4O_{13}]^{2-}$ chains consist of edge-sharing octamolybdate clusters

(*Fig. 3*,*b*), and they are embedded between sheets of irregular M–O-polyhedra (*Figs. 3* and *4*,*a*). For all three compounds, the Mo–O distances are in the usual ranges: the short terminal Mo–O bond lengths (min. 1.67(3) Å) indicate double bonding. The Mo–O bond length continuously increases with the O-coordination number. Among the two-coordinate O-atoms, O(11) exhibits a rather asymmetric distribution of bond lengths: whereas the short Mo–O bond to Mo(3) (*e.g.*, 1.741(3) Å for $Cs_2Mo_4O_{13}$) resembles a terminal distance, the contact to Mo(1) is elongated (*e.g.*, 2.340(3) Å for $Cs_2Mo_4O_{13}$). For a more detailed discussion of Mo–O bond lengths, *cf. Sect. 4.5.3*. The closest M–M distance increases from K (4.006 Å) to Rb (4.201 Å) but *decreases* again for Cs (4.177(1) Å). This minimum Cs–Cs distance is shorter than the typical values for polymolybdates(VI) (4.3–4.8 Å). The coordination number of the alkali cations increases from 8 in *t*-$K_2Mo_4O_{13}$ to 9 in *t*-$Cs_2Mo_4O_{13}$. The bond valence sum (BVS) for both caesium cations (1.219 and 1.274) are considerably higher than those of the corresponding potassium cations (1.080 and 1.082). Both Cs^+ ions are bound to three different $[Mo_4O_{13}]^{2-}$ chains: Cs(1) shares three contacts with each of the chains, whereas Cs(2) is bound to two O-atoms of the first chain, three O-atoms of the second

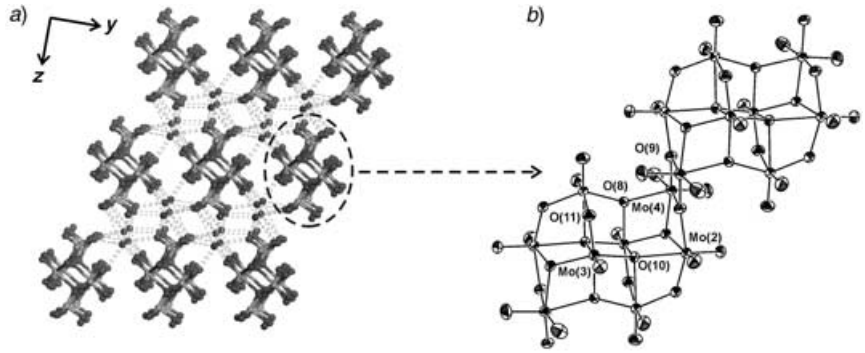

Fig. 3. *Crystal structure of $Cs_2Mo_4O_{13}$:* a) *Perspective view down the [100] direction of the structure, emphasizing the interaction between the $[Mo_4O_{13}]^{2-}$ chains and the Cs^+ cations.* b) *View of the $[Mo_4O_{13}]^{2-}$ chain* (70% probability thermal ellipsoids)

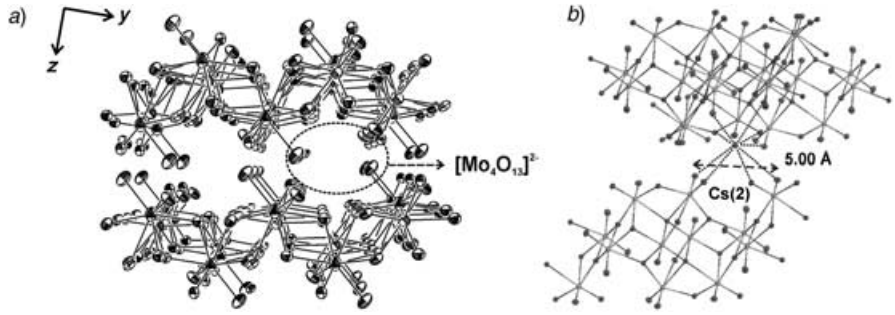

Fig. 4. *Crystal structure of the $M_2Mo_4O_{13}$ tetramolybdates* (M = Rb, Cs): a) *View of the arrangement of Rb–O polyhedra along the [100] direction, emphasizing the position of the $[Mo_4O_{13}]^{2-}$ chains* (70% probability thermal ellipsoids). b) *Environment of Cs(2) in $Cs_2Mo_4O_{13}$* (90% thermal ellipsoids)

Table 1. *Crystallographic Data and Structure Refinement for $Cs_2Mo_4O_{13}$, $Rb_2Mo_4O_{13}$, and $(NH_4)_{0.13}Cs_{1.87}Mo_3O_{10}\cdot H_2O$*

Empirical formula	$Cs_2Mo_4O_{13}$	$Rb_2Mo_4O_{13}$	$(NH_4)_{0.13}Cs_{1.87}Mo_3O_{10}\cdot H_2O$
M/amu	857.58	762.70	714.42
Temperature/K	293(2)	293(2)	295(2)
$\lambda(Mo_{K\alpha})$/Å	0.71073	0.71073	0.71073
Crystal system	triclinic	triclinic	orthorhombic
Space group	*P*-1	*P*-1	*Pnma*
Volume/10^6 pm^3	637.3(1)	595.78(8)	1199.7(4)
Unit cell dimensions:			
a/Å	8.408(1)	8.272(1)	10.221(2)
b/Å	8.652(1)	8.412(1)	7.612(2)
c/Å	10.406(1)	10.288(1)	15.422(3)
α/°	106.10(2)	104.545(2)	
β/°	103.68(2)	106.425(2)	
γ/°	109.76(2)	109.915(2)	
Z	2	2	2
ρ_{calc}/g cm^{-3}	4.469	4.252	3.956
$\mu(MoK_\alpha)$/mm^{-1}	9.53	12.29	8.73
Absorption correction	empirical [37]	empirical [37]	numerical [35][36]
Crystal size/mm	0.28 × 0.15 × 0.08, colorless	0.08 × 0.07 × 0.3, colorless	0.3 × 0.025 × 0.025, colorless
θ range/°	$2.19 \le \theta \le 33.86$	$2.24 \le \theta \le 33.69$	$2.39 \le \theta \le 23.98$
Index ranges	$-12 \le h \le 12$, $-13 \le k \le 13$, $-15 \le l \le 15$	$-12 \le h \le 12$, $-12 \le k \le 13$, $-15 \le l \le 15$	$-11 \le h \le 11$, $-8 \le k \le 8$, $-17 \le l \le 17$
Reflections collected	10002	9222	7299
Independent reflections	4670	4317	1017
Parameters	173	173	89
R_{int}	0.0436	0.0644	0.1351
Refinement method	full matrix least squares on F^2	full matrix least squares on F^2	full matrix least squares on F^2
R_1, wR_2[a])[b]) ($I > 2\sigma(I)$)	0.0273, 0.0484	0.0339, 0.0636	0.0326, 0.0566
R_1, wR_2 (all data)	0.0379, 0.0495	0.0580, 0.0655	0.0653, 0.0636
$\Delta\rho_{max.}$/e Å^{-3}	1.196	1.981	1.070
$\Delta\rho_{min.}$/e Å^{-3}	−2.014	−1.938	−1.041
G.o.f. (F^2)	0.758	0.727	0.981
Extinction coefficient	0.0048(1)	0.0017(1)	–

[a]) $R_1 = \Sigma \| F_o | - | F_c \| / \Sigma | F_o |$. [b]) $wR_2 = \sqrt{\left[\sum \left\{ w\left(F_o^2 - F_c^2\right)^2 \right\} \Big/ \sum \left\{ w\left(F_o^2\right)^2 \right\}\right]}$.

chain, and four O-atoms of the fourth chain. The latter is bound to Cs(2) in a 'chelate-like' fashion over a distance of 5 Å (*Fig. 4,b*).

Both the short minimum Cs–Cs distance and the strong interaction of the Cs^+ cations with the $[Mo_4O_{13}]^{2-}$ chains indicate that the latter might be the dominating structural element. Is this valid for the alkali trimolybdate hydrates as well?

4.3. *Crystal Structure of $(NH_4)_{0.13}Cs_{1.87}Mo_3O_{10}\cdot H_2O$.* 4.3.1. *Trends among the Alkali Trimolybdate Monohydrates.* $[Mo_3O_{10}]^{2-}$ Chains (*Fig. 5,b*) are the common structural motif of the alkali trimolybdate hydrates (*Table SI-1*). Their crystal structures are determined by the size of the alkali cation (*cf. Sect. 4.2.1*): the $[Mo_3O_{10}]^{2-}$ chains in $Na_2Mo_3O_{10}\cdot 3\,H_2O$ [55] are disordered, and the trihydrate structure of $K_2Mo_3O_{10}\cdot 3\,H_2O$ [56] differs from the homotypic pair $Rb_2Mo_3O_{10}\cdot H_2O$ [57] and $Cs_2Mo_3O_{10}\cdot H_2O$ [58]. Previous structure determinations of $Na_2Mo_3O_{10}\cdot 3\,H_2O$ and $K_2Mo_3O_{10}\cdot$

Table 2. *Selected Atom Distances* [Å] *and BVS Values for the* t-$M_2Mo_4O_{13}$ (M = K–Cs) *Series*

Structural feature	M = K [24]	M = Rb (this work)	M = Cs (this work)
Mo–O distance ranges:			
terminal Mo–O	1.67(3) – 1.75(3)	1.692(4) – 1.727(4)	1.694(3) – 1.719(3)
μ_2-O	1.71(3) – 2.35(3)	1.745(4) – 2.347(4)	1.741(3) – 2.340(3)
μ_3-O	1.85(3) – 2.35(3)	1.892(4) – 2.263(3)	1.890(3) – 2.305(3)
μ_4-O	1.95(3) – 2.39(3)	1.923(3) – 2.424(3)	1.920(3) – 2.442(3)
Mo–Mo (intrachain) range:	3.201 – 4.008	3.212 – 4.021	3.209(1) – 4.018(1)
M–O features:			
min. M–M distance	4.006	4.201	4.177(1)
M–O distance range (M(1))	2.69(3) – 3.27(3)	2.810(4) – 3.363(4)	2.994(3) – 3.601(3)
M–O distance range (M(2))	2.67(3) – 3.37(4)	2.819(4) – 3.341(4)	2.980(3) – 3.360(3)
average M–O distance (M(1))	2.90	3.03	3.20
average M–O distance (M(2))	2.93	3.01	3.16
BVS (M(1)), coordination	1.080, 8-fold	1.139, 8-fold	1.219, 9-fold
BVS (M(2)), coordination	1.082, 8-fold	1.207, 8-fold	1.274, 9-fold

3 H_2O were only based on XRD powder data [55][56]. The growth of suitable large single crystals of $Rb_2Mo_3O_{10} \cdot H_2O$ [57] and $Cs_2Mo_3O_{10} \cdot H_2O$ is extremely difficult. This applied as well for our solvothermal routine (*Figs. 1* and *2*).

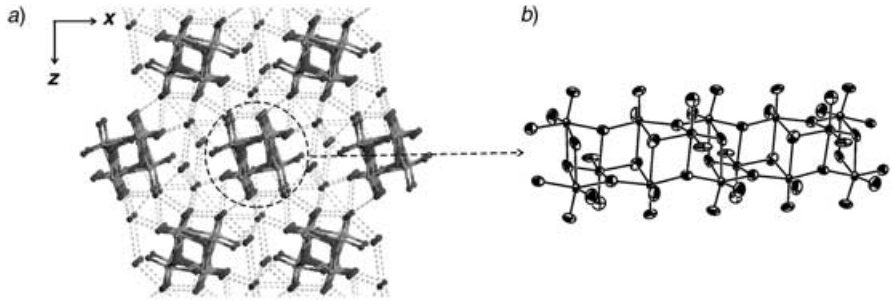

Fig. 5. a) *Perspective view of the structure of* $Cs_2Mo_3O_{10} \cdot H_2O$ *along the [010] direction, displaying the interaction of the* $[Mo_3O_{10}]^{2-}$ *chains and the* Cs^+ *cations.* b) *View of the* $[Mo_3O_{10}]^{2-}$ *chain* (70% probability thermal ellipsoids)

4.3.2. *Structural Features of* $Rb_2Mo_3O_{10} \cdot H_2O$ *and* $(NH_4)_{0.13}Cs_{1.87}Mo_3O_{10} \cdot H_2O$. Details concerning the structure determination of $(NH_4)_{0.13}Cs_{1.87}Mo_3O_{10} \cdot H_2O$ are summarized in *Tables 1* and *3*. The crystal-water positions are only half occupied, and the M(1) position contains 13 mol-% NH_4^+. All Mo–O distances are in the typical ranges (*Table 3*). The structure refinement for $Cs_2Mo_3O_{10} \cdot H_2O$ with a M(1) position fully occupied by Cs led to higher R values, *i.e.*, to ($R = 0.0728$ and $R_w = 0.0970$, (*cf. Table 1*) and larger thermal parameters for M(1) ($U_{eq}(Cs(1)) = 0.0313(4)$, $U_{eq}(M(1)) = 0.0239(5)$) so that we have selected the mixed NH_4/Cs-containing structure model for discussion, keeping in mind that there might still be other options such as a partial occupation of the caesium positions due to a protonation of the Mo–O framework or of the crystal-water molecules.

Table 3. *Selected Atom Distances* [Å] *and BVS Values for* $Rb_2Mo_3O_{10}\cdot H_2O$ *and* $(NH_4)_{0.13}Cs_{1.87}Mo_3O_{10}\cdot H_2O$

Structural feature	M = Rb [57]			M = NH_4, Cs (this work)		
Mo–O distance ranges:						
terminal Mo–O	1.68(1)	–	1.72(1)	1.697(7)	–	1.709(7)
μ_3-O	1.94(1)	–	2.24(1)	1.929(7)	–	2.283(9)
Mo–Mo (intrachain) range:	3.263	–	3.814	3.271(1)	–	3.813(2)
M–O features:						
min. M–M distance	4.766			4.784(1)		
M–O distance range (M(1))	2.86(2)	–	3.06(2)	3.024(7)	–	3.734(9)
M–O distance range (M(2))	2.86(5)	–	3.19(3)	3.11(2)	–	3.637(7)
average M–O distance (M(1))	2.91			3.596		
average M–O distance (M(2))	3.09			3.320		
BVS (M(1)), coordination	1.211, 7			1.394, 10		
BVS (M(2)), coordination	0.794, 7			0.877, 9		

The rigid $[Mo_3O_{10}]^{2-}$ chains exert a strain upon the large Cs^+ cations: the minimum M–M distance in $(NH_4)_{0.13}Cs_{1.87}Mo_3O_{10}\cdot H_2O$ (4.784(1) Å) remains almost unchanged with respect to $Rb_2Mo_3O_{10}\cdot H_2O$ (4.766 Å). The same trend is found among the *t*-$M_2Mo_4O_{13}$ tetramolybdates (*Table 2*). Both rubidium cations in $Rb_2Mo_3O_{10}\cdot H_2O$ are 7-fold coordinated [57], whereas the analogous cations in $(NH_4)_{0.13}Cs_{1.87}Mo_3O_{10}\cdot H_2O$ are 10-fold (M(1)) and 9-fold coordinated (Cs(2)). M(1) completes its coordination sphere with two additional contacts to the crystal-water molecules and a fourth weak contact at 3.734(9) Å to O(1) (*Fig. 6,a*). Compared to Rb(2), Cs(2) contacts one of the Mo–O chains at two extra sites (*Fig. 6,b*). Both compounds display a striking imbalance in the BVS values (*Table 3*): whereas the M(1) positions are tightly bound to the Mo–O framework with a BVS considerably higher than unity, the corresponding values for the M(2) cations decrease sharply to 0.79 (Rb(2)) and 0.88 (Cs(2)), respectively. As a result, Cs(2) displays largest thermal parameters of all atoms in $Cs_2Mo_3O_{10}\cdot H_2O$ (crystal water exempted, $U_{eq}(Cs(2)) = 0.399(3)$). M(1) shares its closest contacts with three different $[Mo_3O_{10}]^{2-}$ chains and mainly contributes to intrachain bonding as indicated by its high BVS of 1.39 (*Fig. 5,a*). Cs(2), on the other hand, 'dissipates' its closest contacts to the crystal-water molecules, and the remaining M–O contacts are distributed among two instead of three chains (*Fig. 6,b*).

The insufficient crystal growth (small needles of poor quality) of both $Rb_2Mo_3O_{10}\cdot H_2O$ and $(NH_4)_{0.13}Cs_{1.87}Mo_3O_{10}\cdot H_2O$ points to structural strains, and these inherent problems are underscored by the BVS mismatch between the cationic positions.

4.4. *Crystal Structure of* $(NH_4)_{0.37}Rb_{5.63}Mo_7O_{24}\cdot 4\,H_2O$. 4.4.1. *Trends among the Heptamolybdates.* Among the alkali/ammonium heptamolybdates, the characteristic $[Mo_7O_{24}]^{6-}$ cluster (*Fig. 7,b*) comes along in three different structure types (*Table SI-3*). Their symmetry decreases with increasing size of the cation: $Na_6Mo_7O_{24}\cdot 14\,H_2O$ [59] adopts an orthorhombic structure, whereas the homotypic $M_6Mo_7O_{24}\cdot 4\,H_2O$ series (M = K [60], Rb, NH_4 [60]) exhibits monoclinic symmetry. Finally, the larger Cs^+ cation prefers a triclinic structure ($Cs_6Mo_7O_{24}\cdot 7\,H_2O$ [61]). Surprisingly, no crystal-structure determination has been performed up to now for $Rb_6Mo_7O_{24}\cdot 4\,H_2O$.

4.4.2. *Structural Features of the* $M_6Mo_7O_{24}\cdot 4\,H_2O$ (M = K, Rb, NH_4) *Series.* Synthetic and structural details for $(NH_4)_{0.37}Rb_{5.63}Mo_7O_{24}\cdot 4\,H_2O$ can be found in

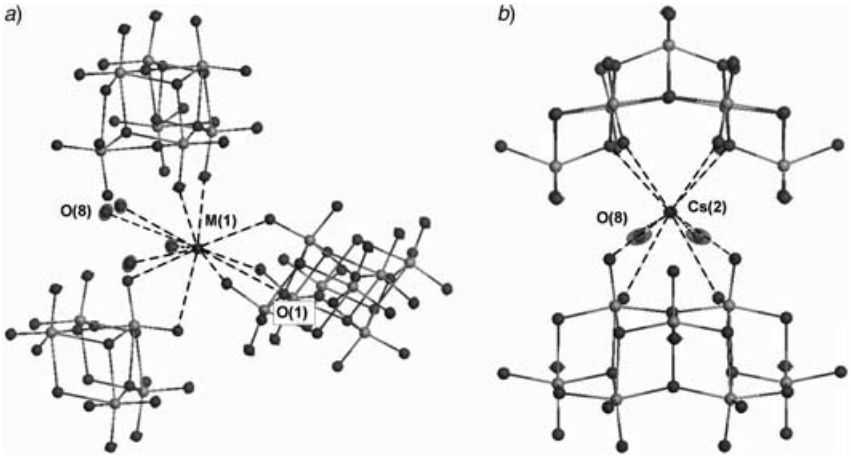

Fig. 6. a) *Environment of Cs(1) in* $Cs_2Mo_3O_{10}\cdot H_2O$ (90% thermal ellipsoids). b) *Environment of Cs(2) in* $Cs_2Mo_4O_{13}\cdot H_2O$ (90% thermal ellipsoids)

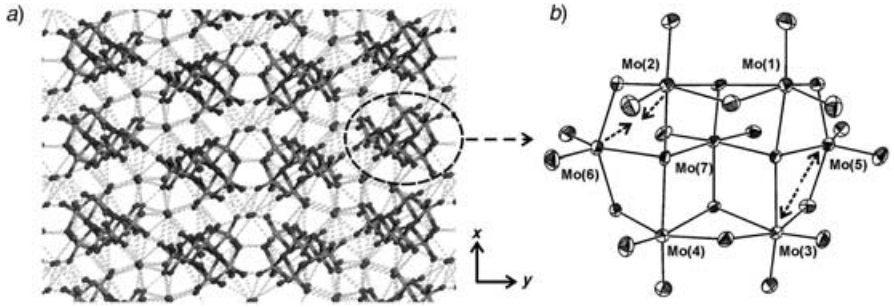

Fig. 7. a) *Crystal structure of* $Rb_6Mo_7O_{24}\cdot 4\,H_2O$ *projected along [001].* b) *Asymmetric distribution of Mo–Mo distances (*dashed arrows*) in the heptamolybdate cluster* (70% probability thermal ellipsoids)

Tables 4 and *5*. The majority of the ammonium cations is located in the M(2) position (20%), whereas the M(3), M(4), and M(6) positions contain less NH_4^+ (between 4 and 7%). Like in the case of $(NH_4)_{0.13}Cs_{1.87}Mo_3O_{10}\cdot H_2O$ (*Sect. 4.3*), the R values for $Rb_6Mo_7O_{24}\cdot 4\,H_2O$ with all cationic positions fully occupied by Rb are larger ($R=0.0497$, $R_w=0.1155$), as well as the thermal parameter for M(2) ($U_{eq}(Rb(2))=0.0432(3)$, $U_{eq}(M(2))=0.294(4)$). Although the partial substitution of Rb^+ by NH_4^+ is a plausible model for the following discussion, other descriptions – such as a Rb deficiency caused by partially protonated heptamolybdate clusters or crystal-water molecules – may still be an option. The monoclinic heptamolybdates (*Table SI-3*) exhibit an almost perfect cleavage parallel to (010) due to the presence of molecular layers that are strongly linked by the cations ('cemented together') [60], whereas the adjacent double layers are only weakly bound. The M(3) position is essential for the interlayer bonding. K(3) distributes its eight M–O contacts exclusively among four different heptamolybdate clusters with no crystal-water molecules attached. Despite its key position, K(3) exhibits the *lowest* BVS of all K^+ cations (0.926), and the same

Table 4. *Crystallographic Data and Structure Refinement for $(NH_4)_{0.37}Rb_{5.63}Mo_7O_{24}\cdot 4\ H_2O$ and $Rb_6Mo_8O_{26}F_2\cdot 6\ H_2O$*

Empirical formula	$(NH_4)_{0.37}Rb_{5.63}Mo_7O_{24}\cdot 4\ H_2O$	$Rb_6Mo_8O_{26}F_2\cdot 6\ H_2O$
M/amu	1605.7	1830.34
Temperature/K	295(2)	293(2)
$\lambda(Mo_{K\alpha})$/Å	0.71073	0.71073
Crystal system	monoclinic	triclinic
Space group	$P2_1/c$	P-1
Volume/10^6 pm^3	2878(1)	835(1)
Unit cell dimensions		
a/Å	8.373(2)	8.233(1)
b/Å	36.347(7)	10.505(1)
c/Å	10.194(2)	10.600(1)
α/°	90	101.86(1)
β/°	111.95(3)	108.78(1)
γ/°	90	96.15(1)
Z	4	1
ρ_{calc}/g cm^{-3}	3.705	3.642
$\mu(Mo_{K\alpha})$/mm^{-1}	12.50	11.71
Absorption correction	empirical [37]	empirical [37]
Crystal size/mm	$0.38\times 0.22\times 0.11$, colorless	$0.28\times 0.07\times 0.04$, colorless
θ range/°	$1.12\le\theta\le 32.10$	$2.02\le\theta\le 33.87$
Index ranges	$-11\le h\le 12$,	$-12\le h\le 12$,
	$-52\le k\le 49$,	$-15\le k\le 16$,
	$-14\le l\le 14$	$-16\le l\le 15$
Reflections collected	32486	13112
Independent reflections	8503	6129
Parameters	371	218
R_{int}	0.1169	0.0592
Refinement method	full matrix least squares on F^2	full matrix least squares on F^2
R_1, wR_2[a])[b]) ($I>2\sigma(I)$)	0.0455, 0.0828	0.0366, 0.0670
R_1, wR_2[a])[b]) (all data)	0.0899, 0.0910	0.0775, 0.0717
$\Delta\rho_{max}$/e Å^{-3}	1.579	1.243
$\Delta\rho_{min}$/e Å^{-3}	−1.920	−1.218
G.o.f. (F^2)	0.897	0.793
Extinction coefficient	0.00143(6)	0.0034(1)

[a]) $R_1=\Sigma\|F_o|-|F_c\|/\Sigma|F_o|$. [b]) $wR_2=\sqrt{\left[\sum\left\{w(F_o^2-F_c^2)^2\right\}/\sum\left\{w(F_o^2)^2\right\}\right]}$.

applies to the 8-fold coordinated M(3) position in $(NH_4)_{0.37}Rb_{5.63}Mo_7O_{24}\cdot 4\ H_2O$ (0.915) (*Fig. 8,a*). This 'cementing' position is, therefore, rather weakly bound, and M(3) displays the largest thermal parameters of all atoms (crystal-water molecules exempted).

Among several structure determinations of $(NH_4)_xRb_{6-x}Mo_7O_{24}\cdot 4\ H_2O$ ($x<0.4$), the data set with optimum R values has been selected for publication. It displays an unusual Mo–Mo distance distribution within the heptamolybdate cluster: the value for Mo(2)–Mo(6) is shortened (3.102(1) Å), whereas the opposite Mo(3)–Mo(5) distance (3.354(2) Å) is significantly extended with respect to the corresponding values for the potassium (3.147 and 3.207 Å) and the ammonium compounds (3.195 and 3.179 Å). M(3) shares most of its 'cementing' M–O contacts (including the four

Table 5. *Selected Atom Distances* [Å] *and BVS Values for the Monoclinic* $M_6Mo_7O_{24}\cdot 4\,H_2O$ *Series* (M = NH_4, K, Rb)

Structural feature	M = NH_4 [60]	M = K [60]	M = Rb, NH_4 (this work)
Mo–O distance ranges:			
terminal Mo–O	1.708(9) – 1.76(1)	1.68(5) – 1.82(4)	1.647(5) – 1.770(5)
μ_2-O	1.73(1) – 2.554(9)	1.60(6) – 2.62(4)	1.871(5) – 2.027(5)
μ_3-O	1.888(9) – 2.260(9)	1.90(4) – 2.28(5)	1.893(4) – 2.307(5)
μ_4-O	2.152(9) – 2.25(1)	2.10(5) – 2.27(4)	2.084(4) – 2.311(5)
Mo–Mo (intracluster) range:	3.179 – 3.463	3.147 – 3.464	3.102(1) – 3.523(2)
M–O features:			
min. M–M distance	3.824	3.685	3.914(2)
M–O distance range	2.74(2) – 3.58(2)	2.72(4) – 3.45(5)	2.703(5) – 3.420(5)
BVS (M(1)), CN, av.dist.	–, 9, 3.05	1.068, 9, 2.94	1.041, 9, 3.085
BVS (M(2)), CN, av.dist.	–, 9, 3.09	1.209, 9, 2.97	1.270, 8, 3.007
BVS (M(3)), CN, av.dist.	–, 8, 3.07	0.926, 8, 2.99	0.915, 8, 3.108
BVS (M(4)), CN, av.dist.	–, 9, 3.04	0.982, 9, 2.97	1.116, 9, 3.053
BVS (M(5)), CN, av.dist.	–, 9, 3.07	1.103, 9, 2.98	1.086, 9, 3.084
BVS (M(6)), CN, av.dist.	–, 10, 3.11	1.259, 10, 3.01	1.276, 8, 2.979

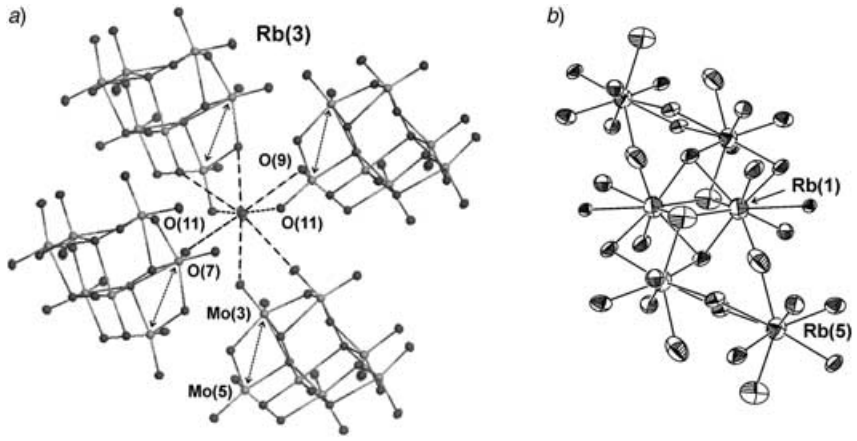

Fig. 8. a) *Coordination of Rb(3) in* $Rb_6Mo_7O_{24}\cdot 4\,H_2O$. b) *Interconnected coordination polyhedra of Rb(1) and Rb(5) in* $Rb_6Mo_7O_{24}\cdot 4\,H_2O$ (70% probability thermal ellipsoids)

closest distances to O(11), O(7), and O(9)) with O-atoms that are bound to Mo(3) or Mo(5). The misbalance in the Mo–Mo distances (indicated by arrows in *Fig. 7,b*) could thus arise from a strain exerted by M(3) that strives to maintain the interlayer bonding. As a result, the monoclinic $M_6Mo_7O_{24}\cdot 4\,H_2O$ type might provide insufficient coordination facilities for the larger caesium cation that prefers coordination numbers up to 11 in triclinic $Cs_6Mo_7O_{24}\cdot 7\,H_2O$ [61].

4.5. *Crystal Structure of* $Rb_6Mo_6O_{28}F_2\cdot 6\,H_2O$. 4.5.1. *Alkali Fluoromolybdates.* Up to now, $K_2Mo_8O_{26}F_2\cdot 6\,H_2O$ has been the only cluster fluoromolybdate [62]. Six different isomers of the $[Mo_8O_{26}]^{4-}$ octamolybdate isopolyanion have been described (α-, β-, γ-, δ-, ε-, and ξ-form) [63], and $K_6Mo_8O_{26}F_2\cdot 6\,H_2O$ contains the fluorinated γ-$[Mo_8O_{26}]^{4-}$

cluster (*Fig. 9,b*). All other fluoromolybdates are composed of highly fluorinated octahedral building blocks (*Table SI-4*) [64–68]. They must be accessed *via* rather harsh preparative treatments involving the use of HF and/or elevated reaction temperatures. We have now established a quick and convenient HF-free route to the new difluorooctamolybdates $Rb_6Mo_8O_{26}F_2 \cdot 6\,H_2O$ and $Cs_6Mo_8O_{26}F_2 \cdot nH_2O$ (*Fig. 1*). The presence of F-atoms in the products was confirmed by elementary analyses (*cf. Sect. 2*). The size of the alkali cation exerts a crucial structural influence on the difluorooctamolybdates. No sodium difluorooctamolybdates could be characterized, and all obtained phases displayed hitherto unassigned powder diffraction patterns. $K_2Mo_8O_{26}F_2 \cdot 6\,H_2O$ [62] and $Rb_6Mo_8O_{26}F_2 \cdot 6\,H_2O$ are homotypic, whereas $Cs_6Mo_8O_{26}F_2 \cdot nH_2O$ adopts a different, modulated structure that is currently under investigation [69].

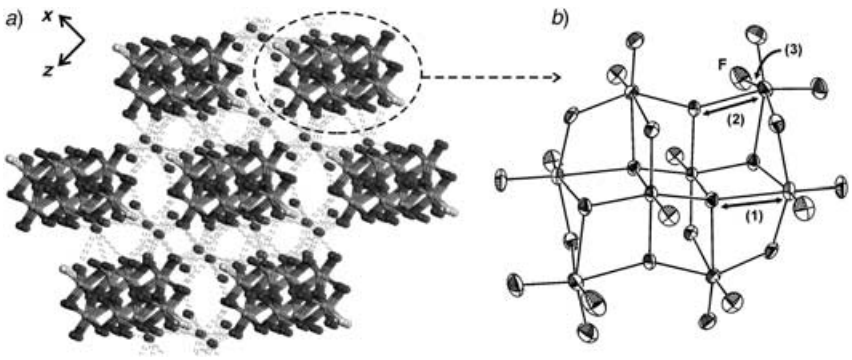

Fig. 9. a) *Perspective view of $Rb_6Mo_8O_{26}F_2 \cdot 6\,H_2O$ along [010]* (the electrostatic interaction between Rb^+ and $[Mo_8O_{26}F_2]^{6-}$ is indicated by dashed lines). b) *View of the difluorooctamolybdate cluster* (70% probability thermal ellipsoids)

4.5.2. *Structural Features of the $M_6Mo_8O_{26}F_2 \cdot nH_2O$ (M = K–Cs) Series. Tables 4* and *6* provide detailed information about the crystal-structure determination of $Rb_6Mo_8O_{26}F_2 \cdot 6\,H_2O$. All Mo–O and Mo–F distances for $K_6Mo_8O_{26}F_2 \cdot 6\,H_2O$ and $Rb_6Mo_8O_{26}F_2 \cdot 6\,H_2O$ are in the same range (*Table 6*). The $[Mo_8O_{26}F_2]^{6-}$ clusters are embedded into a network of irregular Rb–O polyhedra (*Fig. 10,a*). As expected for the larger Rb^+ cation, the coordination numbers of M(2) and M(3) increase from 8 (K^+) to 9 (Rb^+). Each Rb^+ cation is bound to three different difluorooctamolybdate clusters and displays BVS values higher than unity. Nevertheless, their thermal parameters are larger than those of $Rb_2Mo_4O_{13}$ or $(NH_4)_{0.37}Rb_{5.63}Mo_7O_{24} \cdot 4\,H_2O$ (*cf. Appendix*). The minimum Rb–Rb distance in $Rb_6Mo_8O_{26}F_2 \cdot 6\,H_2O$ (4.028(1) Å for Rb(3)–Rb(3)) is slightly *decreased* with respect to the closest K–K distance in $K_6Mo_8O_{26}F_2 \cdot 6\,H_2O$ (4.060 Å). *Fig. 10,b* shows that the Rb(3)–Rb(3) contact is the base diagonal of an Rb–O octahedron consisting of Rb(3), O(2), and O(7). Rb(3) displays maximum thermal parameters (crystal water exempted), and its longest main axis ($U_{11} = 0.051(1)$) is aligned parallel to the opposite Rb(3) to minimize further M–M contact.

Table 6. *Selected Atom Distances* [Å] *and BVS Values for* $M_6Mo_8O_{26}F_2 \cdot 6\,H_2O$ (M = K, Rb) *Difluorooctamolybdates*

Structural feature	M = K [62]			M = Rb (this work)		
Mo–O distance ranges:						
terminal Mo–O	1.703(3)	–	1.724(3)	1.694(4)	–	1.724(3)
μ_2-O	1.755(2)	–	2.408(2)	1.745(3)	–	2.390(3)
μ_3-O	1.882(2)	–	2.291(2)	1.866(3)	–	2.301(3)
μ_4-O	1.971(3)	–	2.398(2)	1.970(3)	–	2.410(3)
$[Mo_8O_{26}F_2]^{6-}$ distances:						
Mo–F distance	1.970(3)			1.972(3)		
Mo–Mo distance range	3.246	–	3.903	3.240(1)	–	3.912(1)
Cationic features:						
min. M–M distance	4.060			4.028(1)		
M–O distance range	2.694(3)	–	3.134(3)	2.829(4)	–	3.500(5)
min. M–F distance	2.671(3)			2.800(3)		
BVS (M(1)), CN, av. distance	1.081,	8 + F,	2.954	1.174,	8 + F,	3.020
BVS (M(2)), CN, av.distance	1.084,	8,	2.888	1.046,	9,	3.090
BVS (M(3)), CN, av. distance	1.161,	8,	2.856	1.188,	9,	3.032

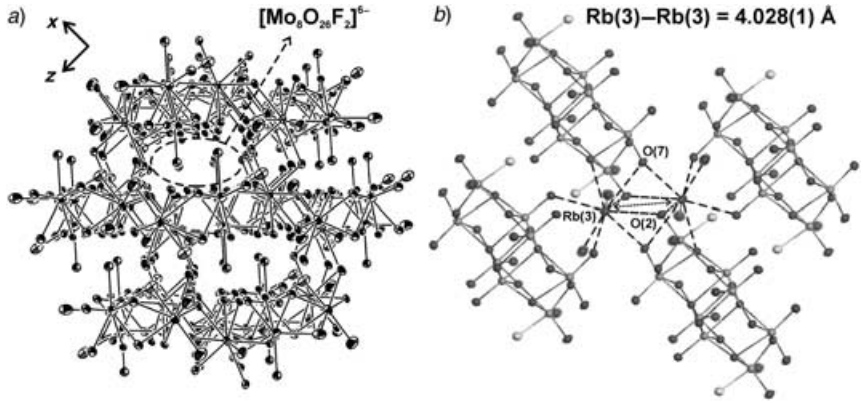

Fig. 10. a) *Perspective view of the Rb/O-polyhedra network along [010], indicating the position of the* $[Mo_8O_{26}F_2]^{6-}$ *clusters.* b) *Environment of Rb(3) in* $Rb_6Mo_8O_{26}F_2 \cdot 6\,H_2O$ (90% probability thermal ellipsoids)

The structure of $Cs_6Mo_8O_{26}F_2 \cdot nH_2O$ is considerably altered. Preliminary results indicate the presence of a monoclinic cell ($P2_1/c$, $a = 11.592(3)$, $b = 19.690(5)$, $c = 8.227(1)$ Å, $\beta = 104.29(1)^\circ$) with a modulation in the c direction [69].

4.5.3. *γ-Octamolybdate-Based Compounds.* According to DF calculations, the stability of the various $[Mo_8O_{26}]^{4-}$ isomers decreases in the following order: α- and δ-forms > ε- and ζ-forms $\gg$ β-form [63]. The γ-cluster should be considered identical to the ζ-form due to an exceptionally elongated Mo–O bond (3.06 Å; indicated as (1) in *Fig. 9*). The γ-isomer is present in $[Me_3N(CH_2)_6NMe_3]_2[Mo_8O_{26}] \cdot 2\,H_2O$ [70], and the addition of two ligands to the γ-cluster affords the substituted $[Mo_8O_{26}L_2]^{2-}$ clusters (*Fig. 9*). Alternatively, the individual γ-clusters can be linked up to chain molybdates *via* common octahedral corners (*e.g.*, in $(NH_4)_6Mo_8O_{27} \cdot 4\,H_2O$) [71] or *via* edges (*e.g.*, in the t-$M_2Mo_4O_{13}$ tetramolybdates, *Sect. 4.2*). The trend among selected Mo–O bond

Table 7. *Selected Mo–O Bond Lengths* [Å] *for the γ-[Mo_8O_{26}]$^{4-}$ Cluster and Its [$Mo_8O_{26}L_2$]$^{6-}$ Derivatives*

	l_1, BO_1	l_2, BO_2	l_3, BO_3, tot. BO	Ref.
Theor. γ-[Mo_8O_{26}]$^{4-}$	3.06, (0.06)	1.92, (0.63)	–	[63]
$[Me_3N(CH_2)_6NMe_3]_2[Mo_8O_{26}]\cdot 2\,H_2O$	2.495(4), 0.18	1.893(4), 0.97	6.08	[70]
$(NH_4)_6Mo_8O_{27}\cdot 4\,H_2O$	2.196(7), 0.40	2.196(7), 0.40	1.889(7), 0.98, 5.87	[71]
$(C_3H_{10}N_6)[H_2Mo_8O_{26}]\cdot 2\,H_2O$	2.233(5), 0.36	2.138(6), 0.47	1.972(7), 0.76, 5.75	[72]
$(C_5H_5NH)_4[(C_5H_5N)_2Mo_8O_{26}]\cdot 2Me_2SO$	2.272(3), 0.32	2.111(3), 0.50	2.279(5), 0.32, 5.78	[73]
$K_6[Mo_8O_{26}(NCS)_2]\cdot 6\,H_2O$	2.248(4), 0.34	2.123(4), 0.49	2.143(4), 0.46, 5.81	[74]
$[NH_3(C_3H_7)]_6[Mo_8O_{28}(CHO)_2]$	2.282(3), 0.31	2.068(3), 0.57	2.124(3), 0.48, 6.02	[75]
$K_6Mo_8O_{26}F_2\cdot 6\,H_2O$	2.217(2), 0.37	2.133(2), 0.47	1.970(3), 0.76, 6.00	[62]
$Rb_6Mo_8O_{26}F_2\cdot 6\,H_2O$	2.217(3), 0.37	2.149(3), 0.45	1.972(3), 0.76, 6.13	this work
$K_2Mo_4O_{13}$	2.23(3), 0.36	2.30(3), 0.30	1.92(3), 0.89, 5.68	[24]
$Rb_2Mo_4O_{13}$	2.276(3), 0.32	2.263(3), 0.33	1.945(3), 0.82, 5.73	this work
$Cs_2Mo_4O_{13}$	2.296(3), 0.30	2.262(3), 0.33	1.939(3), 0.84, 5.90	this work

distances of γ-cluster-based molybdates is in line with the theoretically predicted bond elongation (*Table 7*) [72–75]: the naked γ-cluster by far displays the longest 'critical' Mo–O distance ($(1) = l_1 = 2.495(4)$ Å, *cf. Table 7, Entry 2*) of all compounds. Moreover, its Mo–O bond (2) (*Fig. 9*) is considerably shortened with respect to all reference compounds ($(2) = l_2 = 1.893(4)$ Å; *cf. Table 7, Entry 2*). In this way, the expected bond order ($BO = 6.08$) is maintained at the pentacoordinate Mo(2). Among the substituted compounds, only $Rb_6Mo_8O_{26}F_2\cdot 6\,H_2O$ displays a higher bond order for Mo(2) ($BO = 6.13$). The unsymmetric Mo–O bond-length distribution within the γ-cluster is straightened out by ligand uptake and chain formation.

5. High-Throughput Investigation on Mixed Alkali Systems. – The Cs^+ compound often adopts a special structure among a series of alkali polymolybdates(VI) (see *Sect. 4.4* and *4.5*). The (rather limited) data on mixed alkali polymolybdates confirm this trend [76]. We have, therefore, monitored the onset of structural changes as a function of the cation ratio in mixed Rb/Cs polymolybdates(VI). High-throughput solvothermal techniques [25–29] were applied for a preliminary screening of the MX/M′X/$MoO_3\cdot 2\,H_2O$ (M = Rb, M′ = Cs, X = F, I) systems in acidic media. The mixed iodides fail to afford crystalline polymolybdates(VI), and mixed hexagonal molybdates are formed instead (*Fig. 11,a*). In contrast to the highly reductive iodides, the corresponding mixed fluoride systems readily yield mixed crystalline Rb/Cs tetramolybdates in the presence of acetic acid (AcOH). Rb/Cs Difluorooctamolybdates (accompanied by residual amounts of mixed tetramolybdates) are accessible in the presence of 0.1M HCl (*Fig. 11*). Depending on the Rb/Cs ratio in the starting material, three different types of mixed difluorooctamolybdates were observed: both $Rb_6Mo_8O_{26}F_2\cdot 6\,H_2O$ of the *P*-1 type (*cf. Sect. 4.5.2*) and $Cs_6Mo_8O_{26}F_2\cdot nH_2O$ of the modulated type (*cf. Sect. 4.5.2*) dissolve limited amounts of the other cation to yield $Rb_{6-x}Cs_xMo_8O_{26}F_2\cdot 6\,H_2O$ ($0 < x < 0.54$) and $Cs_{6-x}Rb_xMo_8O_{26}F_2\cdot nH_2O$ ($0 < x < 0.24$). Between these two solid solutions, $Rb_3Cs_3Mo_8O_{26}F_2\cdot nH_2O$ emerges as a novel, discrete difluorooctamolybdate phase ($P2_1/n$, $a = 8.123(1)$, $b = 14.737(2)$, $c = 13.388(2)$ Å, $\beta = 95.872°$, the complete structural description will be provided in a follow-up study on new mixed alkali molybdates) [77]. The miscibility behavior of the Rb/Cs difluoro-

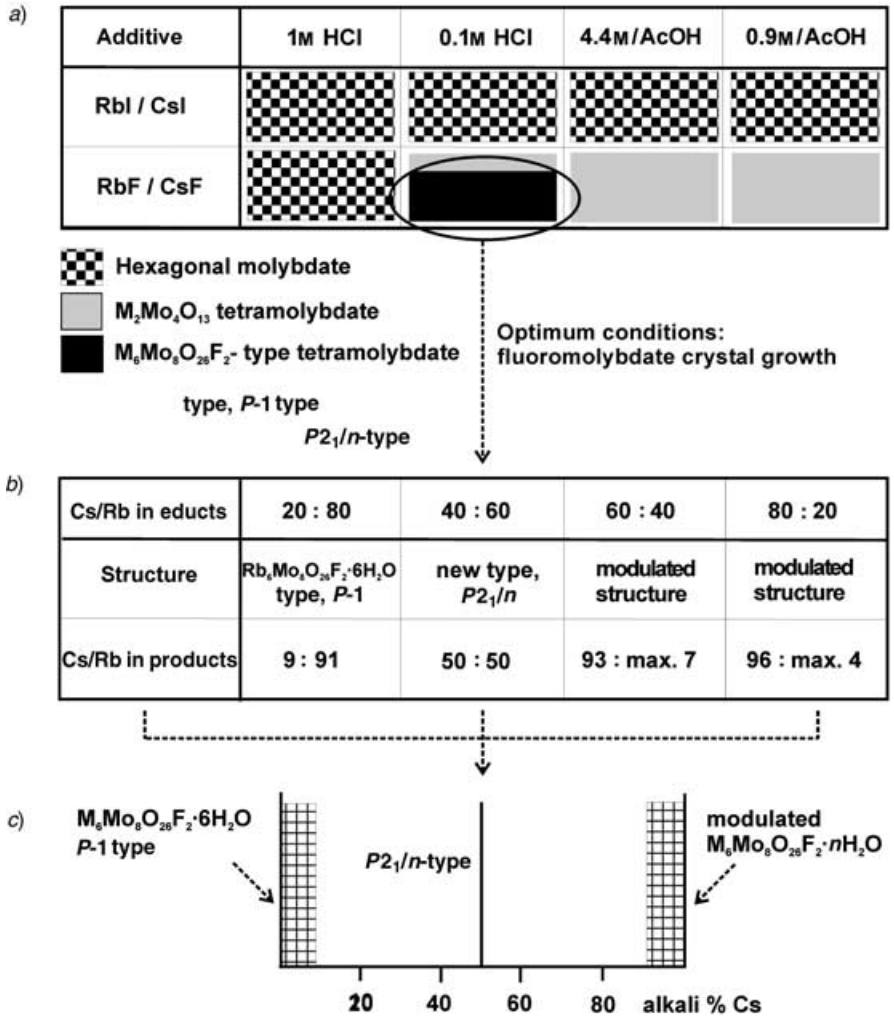

Fig. 11. a) *Selected high-throughput experiments revealing optimum conditions for mixed fluoromolybdate formation from* $MoO_3 \cdot 2\,H_2O$ *and RbF/CsF.* b) *Structure type and cation ratios in the emerging mixed difluorooctamolybdates.* c) *Miscibility behavior of* $Rb_6Mo_8O_{26}F_2 \cdot 6\,H_2O$ *and* $Cs_6Mo_8O_{26}F_2 \cdot n H_2O$

octamolybdate system is typical of nonisostructural oxides: the mutual solubility is low, so that a ternary 1:1 compound is formed instead of a solid solution (for exper. details, *cf. Sect. 2*).

6. Discussion. – 6.1. *Preparative Guidelines.* The applied synthetic pathway is often crucial for the crystal structures of polymolybdates(VI), as illustrated by the manifold modifications of $Cs_2Mo_4O_{13}$: the long sought-after *t*-$Cs_2Mo_4O_{13}$ cannot be accessed by solid-state techniques so that it was finally found *via* solvothermal methods. Generally,

the latter provide a straightforward access to crystalline rubidium and caesium poly(fluoro)molybdates(VI) starting from Mo-based precursors and alkali halides. The following synthetic guidelines could be derived from the present study:

1) The structure of the molybdenum-containing educt may be decisive for addressing a desired molybdate. Tri- and heptamolybdates, *e.g.*, were exclusively available from the cluster compound ammonium heptamolybdate as a precursor material (*Sect. 3*) due to its special solvothermal reactivity that differs from the topotactically related series MoO_3, $MoO_3 \cdot 0.33\,H_2O$, and $MoO_3 \cdot 2\,H_2O$. Although ammonium heptamolybdate is a convenient educt for the screening of solvothermal fields, the possible incorporation of ammonium cations into the products (*cf. Sect. 4.3* and *4.4*) should be circumvented by the use of alkali heptamolybdates for synthetic purposes. More general precursor–structure relationships would be quite useful for predictive solvothermal syntheses.

2) The influence of the halide ion on the solvothermal process is crucial as well. Both iodides and fluorides actively participate in the reaction: whereas the reducing activity of iodides triggers the formation of by-products (hexagonal molybdates) or $M_{0.33}MoO_3$ bronzes (*Fig. 2*), fluorides readily afford novel difluorotetra- and difluorooctamolybdates. The close structural relation of difluorotetra- and difluorooctamolybdates *via* the γ-$[Mo_8O_{26}]^{4-}$ cluster as a common structural motif illustrates that fluoride anions and alkali cations are equally important solvothermal synthetic tools. When the reaction temperature is raised from 100 to 180°, the fluoride anions fluorinate the $[Mo_4O_{13}]^{2-}$ chains (*Fig. 3*) of the alkali tetramolybdates like 'chemical scissors' and cut them up into discrete $[Mo_8O_{26}F_2]^{6-}$ units (*Fig. 9*). Longer solvothermal treatments (6 d) finally break up the octamolybdate clusters into the highly fluorinated, isolated $[O_2FMoO_2FMoO_2F]^{3-}$ ions of $Cs_3Mo_2O_6F_3$ (*Table SI-4*).

3) The solvothermal routines are rather robust towards minor parameter fluctuations in reaction time (1–5 d) and temperature (*ca.* ± 10–15°). The latter can be employed on a larger scale (± 80°) to control the structure of the emerging molybdates: *Rb/Cs tetramolybdates are best prepared starting from MoO_3-related precursors and RbF/CsF at 100°. Elevated reaction temperatures (220°) afford fluoromolybdates.*

Hand in hand with systematic synthetic fields and high-throughput methods, we furthermore apply *in situ* EXAFS- and XRD techniques to directly monitor the progress of solvothermal reactions [78][79].

6.2. *Structure Trends.* A comparison of the chain-based tri- and tetramolybdates and the cluster-containing difluorohepta- and difluorooctamolybdates shows that both molybdate types react differently towards the introduction of the large Cs^+ cation: whereas the structure type is maintained among the chain-based caesium molybdates (*Table SI-1*), the cluster-based caesium compounds adopt a different packing motif (*Tables SI-3* and *SI-4*). Two questions can now be raised: *i*) How does the anionic molybdate motif of a given structure exactly arrange with the large Cs^+ cation? *ii*) Can the structure-determining potential of Cs^+ be exploited to generate new cluster-based (fluoro)polymolybdates?

The role of the alkali cations in the newly determined crystal structures of the chain molybdates $(NH_4)_{0.13}Cs_{1.87}Mo_3O_{10} \cdot H_2O$, $Rb_2Mo_4O_{13}$, and $Cs_2Mo_4O_{13}$, and in the cluster molybdates $(NH_4)_{0.37}Rb_{5.63}Mo_7O_{24} \cdot 4\,H_2O$, $Rb_6Mo_8O_{26}F_2 \cdot 6\,H_2O$, and $Cs_6Mo_8O_{26}F_2 \cdot nH_2O$ was investigated from this perspective (*cf. Sect. 4*).

i) *Chain Molybdates:* The molybdate chains are the dominating structural element so that they induce a strain upon the larger alkali cations. Among a given alkali polymolybdate(VI) series, the closest M–M distance usually increases from the K^+ to the Rb^+ compound, and this trend should be continued with Cs^+ due to the increasing difference in ionic radii from Rb^+ to Cs^+ [43]. For both $Cs_2Mo_3O_{10}\cdot H_2O$ and $Cs_2Mo_4O_{13}$, however, the contrary is observed: the minimum M–M distance remains almost constant ($(NH_4)_{0.13}Cs_{1.87}Mo_3O_{10}\cdot H_2O$) or even decreases ($Cs_2Mo_4O_{13}$) with respect to the corresponding rubidium molybdate. This points to a very limited space for the large Cs^+ cations between the molybdate chains. Moreover, $Rb_2Mo_3O_{10}\cdot H_2O$ and $(NH_4)_{0.13}Cs_{1.87}Mo_3O_{10}\cdot H_2O$ display a considerable electrostatic mismatch between the BVS values of the two cationic positions.

These structural misbalances might contribute to the difficulties in preparing $(NH_4)_{0.13}Cs_{1.87}Mo_3O_{10}\cdot H_2O$ and *t*-$Cs_2Mo_4O_{13}$. Both crystal structures were hitherto undetermined, and the trimolybdate crystallizes very poorly. The absence of *t*-$Cs_2Mo_4O_{13}$ was explained in terms of a steric mismatch between the large cation and the rigid $[Mo_4O_{13}]^{2-}$ chains [24]. As *t*-$Cs_2Mo_4O_{13}$ is only accessible under mild solvothermal conditions (100°), it might indeed be metastable with respect to its manifold isomers occurring at higher temperatures (*Table SI-2*). Differential thermal analysis (DTA) investigations of *t*-$Cs_2Mo_4O_{13}$ confirm this assumption [77].

Cluster-Based Molybdates: A comparison of the cationic environment in $(NH_4)_{0.37}Rb_{5.63}Mo_7O_{24}\cdot 4\,H_2O$ and $K_6Mo_7O_{24}\cdot 4\,H_2O$ reveals that the monoclinic structure type does not provide additional Mo–O contacts for the larger Rb^+ cations and might thus be unsuitable for the steric demands of the larger Cs^+ cation that prefers the triclinic structure of $Cs_6Mo_7O_{24}\cdot 7\,H_2O$. Similar issues could lead to the modulation in $Cs_6Mo_8O_{26}F_2\cdot nH_2O$. As the closest M–M distance already *decreases* from $K_6Mo_8O_{26}F_2\cdot 6\,H_2O$ to $Rb_6Mo_8O_{26}F_2\cdot 6\,H_2O$, the triclinic cluster arrangement might finally give way to the larger Cs^+ cation.

Residual Ammonium Cations: The incorporated ammonium cations in both $(NH_4)_{0.37}Rb_{5.63}Mo_7O_{24}\cdot 4\,H_2O$ and $(NH_4)_{0.13}Cs_{1.87}Mo_3O_{10}\cdot H_2O$ exhibit distinct site preferences among the six or two different cationic positions, respectively. This inspired us to study the cation distribution in mixed molybdates, and the resulting trends will be discussed in forthcoming publications [77].

ii) High-throughput screening experiments (*Sect. 5*) revealed that the crystal structure of mixed Rb/Cs-difluorooctamolybdates depends on the cation ratio. Meanwhile, we have expanded this structure-directing approach upon the preparation of further novel alkali fluoromolybdates, such as the first fluorinated *Anderson–Evans* clusters [77]. The newly generated fluoromolybdate family serves as a model system for deriving structure–synthesis guidelines.

7. Conclusion and Perspectives. – The development of predictive concepts in synthetic inorganic chemistry is of crucial importance for modern materials design. Polymolybdates(VI) provide excellent examples for such structure–synthesis relationships so that we have studied the preparation of crystalline rubidium and caesium polymolybdates(VI) in terms of systematic solvothermal fields and high-throughput experiments. The emerging synthetic guidelines provide controlled access to chain and cluster molybdates. The newly determined crystal structures were compared with

respect to the cationic environments, and the results point to a considerable structure-directing potential of the Cs^+ cation. This approach is currently applied upon the targeted synthesis of novel alkali fluoromolybdates.

With the help of newly designed *in situ* EXAFS equipment, the mechanisms of solvothermal molybdate formation will be investigated. Furthermore, an extensive solvothermal and crystallographic study on mixed alkali molybdates is under way. The long-term goals are synthetic protocols for tailor-made molybdate structures.

We thank Prof. *R. Nesper*, Laboratory of Inorganic Chemistry, ETH Zürich, for his steady interest and for the generous benefit. This work was supported by the ETH Zürich, by the *Swiss National Science Foundation* ('*MaNEP – Materials with Novel Electronic Properties*'), and by the *National Research Program* ('*Supramolecular Functional Materials*'). We thank Dr. *M. Wörle*, Laboratory of Inorganic Chemistry, ETH Zürich, for helpful discussions on the results of the present study.

Appendix. – Supplementary information is given in *Tables SI-1* to *SI-4*.

Table 8. SI-1. *Survey of Alkali Trimolybdate Hydrates and Triclinic Alkali Tetramolybdates*

	Space group	Preparation	Ref.
$K_2Mo_4O_{13}$	*P*-1	synthesis from a slowly cooled melt K_2CO_3/MoO_3 1 : 4 ratio	[24]
$Rb_2Mo_4O_{13}$	***P*-1**	**solvothermal treatment of RbI or RbF and Mo-based precursors ($T < 180°$)**	**this work**
$Cs_2Mo_4O_{13}$	***P*-1**	**solvothermal treatment of CsI or CsF and Mo-based precursors ($T < 180°$)**	**this work**
$Na_2Mo_3O_{10} \cdot 3\ H_2O$	*C*2/*m*	growth from solutions of Na_2MoO_4 and $HNO_3/NaNO_3$	[55]
$K_2Mo_3O_{10} \cdot 3\ H_2O$	*Cmcm*	growth from solutions of $K_2MoO_4 \cdot 2\ H_2O$ and HNO_3/KNO_3	[56]
$Rb_2Mo_3O_{10} \cdot H_2O$	*Pnma*	12 d of solvothermal treatment at 70° ($Rb_6Mo_7O_{24} \cdot 4\ H_2O$ and $RbOH \cdot 2\ H_2O$)	[57]
$Cs_2Mo_3O_{10} \cdot H_2O$	***Pnma***	**2 d of solvothermal treatment at 100° ($(NH_4)_6Mo_7O_{24} \cdot 4\ H_2O$ and CsI)**	**this work**

Table 9. SI-2. *Modifications of $Cs_2Mo_4O_{13}$ Reported in the Literature*

Crystallographic data	Structure	Preparation	Ref.
*C*2/*c*, $a = 45.92(5)$, $b = 10.418(3)$, $c = 7.923(8)$ Å, $\beta = 92.94(5)°$	two different infinite $[Mo_4O_{13}]^{2-}_n$ chains along [001]	heating of $Cs_2CO_3/MoO_3/MoO_2$ 1 : 3 : 1 for 12 h at 900 K	[53]
*C*2/*c* or *Cc*, $a = 21.53(4)$, $b = 5.58(2)$, $c = 14.38(3)$ Å, $\beta = 122.8(3)°$	unknown	slow cooling of a Cs_2CO_3/MoO_3 melt	[24]
$a = 10.973(9)$, $b = 18.234(7)$, $c = 7.306(2)$ Å, $\beta = 94.08(4)°$	unknown	thermal treatment of Cs_2MoO_4/MoO_3 1 : 3 under a flow of air	[54]
$a = 11.378(5)$, $b = 14.895(6)$, $c = 9.312(4)$ Å, $\beta = 91.89(3)°$	unknown	thermal treatment of Cs_2MoO_4/MoO_3 1 : 3 under a flow of air	[54]
$a = 17.34(7)$, $b = 16.706(5)$, $c = 4.460(3)$ Å, $\beta = 90.10(5)°$	unknown	thermal treatment of Cs_2MoO_4/MoO_3 1 : 3 under a flow of air	[54]
No information given	unknown, m.p. 534°	thermal treatment of the Cs_2MoO_4/MoO_3 system	[54]

Table 10. SI-3. *Survey of Alkali and Ammonium Heptamolybdates*

	Space group	Synthesis	Ref.
$Na_6Mo_7O_{24}\cdot 14\ H_2O$	$P2_1ab$	evaporation of sodium molybdate solutions in the presence of $HClO_4$	[59]
$K_6Mo_7O_{24}\cdot 4\ H_2O$	$P2_1/c$	evaporation of a MoO_3/KOH solution at pH 6	[60]
$(NH_4)_6Mo_7O_{24}\cdot 4\ H_2O$	$P2_1/c$	growth of single crystals from a solution of ammonium paramolybdate	[60]
$Rb_6Mo_7O_{24}\cdot 4\ H_2O$	***$P2_1/c$***	**hydrothermal treatment of ammonium heptamolybdate with 4M RbI at 220°**	**[80], this work**
$Cs_6Mo_7O_{24}\cdot 7\ H_2O$	*P*-1	addition of CsCl to a solution of sodium molybdate at pH 7	[61]

Table 11. SI-4. *Survey of Alkali Fluoromolybdates*

	Space group	Structural motif	Synthesis	Ref.
$K_6Mo_8O_{26}F_2\cdot 6\ H_2O$	*P*-1	$[Mo_8O_{26}F_2]^{6-}$ cluster	evaporation and redissolution of MoO_3/HF/KOH/H_2O	[62]
$Rb_6Mo_8O_{26}F_2\cdot 6\ H_2O$	***P*-1**	**$[Mo_8O_{26}F_2]^{6-}$ cluster**	**solvothermal treatment of RbF/ Mo-based precursors**	**this work**
$Cs_6Mo_8O_{26}F_2\cdot nH_2O$		**$[Mo_8O_{26}F_2]^{6-}$ cluster, modulated**	**solvothermal treatment of CsF/ Mo-based precursors**	**this work**
$Cs_3Mo_2O_6F_3$	$P6_3/mmc$	isolated ions: $[O_2FMoO_2FMoO_2F]^{3-}$	reaction of CsF and MoO_3 at 600° under O_2	[64]
$CsMoO_2F_3$	*Imma*	*cis* chains: $(MoO_2F_{2/2}F_{2/2})$ octahedra	crystallization from MoO_3/Cs_2CO_3 and 40% HF solution	[65]
$Rb_2MoO_2F_4$	*Amam*	isolated $[MoO_2F_4]$ trigonal bipyramids	–	[66]
$K_2MoO_2F_4\cdot H_2O$	$P2_1/c$	isolated $[MoO_2F_4]^{2-}$ octahedra	–	[67]
$K_2MoOF_5\cdot H_2O$	*C*2	isolated $[MoOF_5]^{2-}$ octahedra	–	[67]
$A_2A'MoO_3F_3$ (A, A′ = K, Rb, Cs)	*Fm*3*m*	elpasolite structure	reaction of alkali fluorides and MoO_3 under Ar (460–900°)	[68]

REFERENCES

[1] K. Byrappa, M. Yoshimura, 'Handbook of Hydrothermal Technology', Noyes, Park Ridge, N.J., 2001.
[2] R. I. Walton, *Chem. Soc. Rev.* **2002**, *31*, 230.
[3] G. Demazeau, *J. Mater. Chem.* **1999**, *9*, 15.
[4] C. N. R. Rao, F. L. Deepak, G. Gundiah, A. Govindaraj, *Prog. Solid State Chem.* **2003**, *31*, 5.
[5] M. Rajamathi, R. Seshadri, *Curr. Opin. Solid State Mater. Sci*. **2002**, *6*, 337.
[6] S. Komarneni, *Curr. Sci.* **2003**, *85*, 1730.
[7] M. S. Whittingham, J.-D. Guo, R. Chen, T. Chirayil, G. Janauer, P. Zavalij, *Solid State Ionics* **1995**, *75*, 257.
[8] G. R. Patzke, F. Krumeich, R. Nesper, *Angew. Chem.*, *Int. Ed.* **2002**, *41*, 2446.
[9] R. I. Walton, F. Millange, R. I. Smith, T. C. Hansen, D. O'Hare, *J. Am. Chem. Soc.* **2001**, *123*, 12547.
[10] A. K. Cheetham, C. F. Mellot, *Chem. Mater.* **1997**, *9*, 2269.
[11] A. Michailovski, F. Krumeich, G. R. Patzke, *Helv. Chim. Acta* **2004**, *87*, 1029.
[12] A. Michailovski, F. Krumeich, G. R. Patzke, *Chem. Mater.* **2004**, *16*, 1433.
[13] G. R. Patzke, A. Michailovski, F. Krumeich, R. Nesper, J.-D. Grunwaldt, A. Baiker, *Chem. Mater.* **2004**, *16*, 1126.
[14] J. Haber, E. Lalik, *Catal. Today* **1997**, *33*, 119.

[15] H.-F. Liu, R.-S. Liu, K. Y. Liew, R. E. Johnson, J. H. Lunsford, *J. Am. Chem. Soc.* **1984**, *106*, 4117.
[16] A. Baiker, P. Dollenmeier, A. Reller, *J. Catal.* **1987**, *103*, 394.
[17] T. Ressler, J. Wienold, R. E. Jentoft, *J. Catal.* **2002**, *210*, 67.
[18] K. Galatsis, Y. X. Li, W. Wlordarski, E. Comini, G. Sberveglieri, C. Catalini, S. Santucci, M. Passacantando, *Sens. Actuators B* **2002**, *83*, 276.
[19] Y. Xu, *Curr. Opin. Solid State Mater. Sci*. **1999**, *4*, 133.
[20] A. Clearfield, *Prog. Cryst. Growth Charact. Mater.* **1991**, *21*, 1.
[21] 'Perspectives in the Solid State Coordination Chemistry of the Molybdenum Oxides', Eds. M. T. Pope and A. Müller, Kluwer Academic Publishers, Dordrecht, 2001.
[22] R. S. Rarig, P. Hagrman, J. Zubieta, *Solid State Sci.* **2002**, *4*, 77.
[23] B. M. Gatehouse, B. K. Miskin, *Acta Crystallogr.*, *Sect. B* **1975**, *31*, 1293; B. M. Gatehouse, B. K. Miskin, *J. Solid State Chem.* **1974**, *9*, 247.
[24] B. M. Gatehouse, P. Leverett, *J. Chem. Soc. A* **1971**, 2107.
[25] N. Stock, T. Bein, *Angew. Chem.*, *Int. Ed.* **2004**, *43*, 749.
[26] N. Stock, T. Bein, *Solid State Sci.* **2003**, *5*, 1207.
[27] N. Stock, N. Hilbrandt, K. Choi, T. Bein, *Stud. Surf. Sci. Catal.* **2001**, *38*, 550.
[28] N. Stock, T. Bein, *Z. Anorg. Allg. Chem.* **2002**, *628*, 2150.
[29] N. Stock, T. Bein, *J. Mater. Chem.* **2005**, *15*, 1384.
[30] J. J. Cruywagen, J. B. B. Heyns, *S. Afr. J. Chem.* **1981**, *34*, 118.
[31] 'INTEGRATE, Version 2.83', Stoe & Cie, Darmstadt, 1997.
[32] 'SAINT Version 4.05', Siemens Analytical X-ray Instruments, Madison, WI, USA, 1996.
[33] 'SHELXTL Version 5.1 Program Package', Bruker AXS, Inc., Madison, WI, USA, 1998.
[34] G. M. Sheldrick, 'SHELX97, Programs for the Refinement of Crystal Structures', Göttingen, 1997.
[35] 'X-RED 1.07, Data Reduction for STADI4 and IPDS', Stoe & Cie, Darmstadt, 1996.
[36] 'X-SHAPE 1.01, Crystal Optimisation for Numerical Absorption Correction', Stoe & Cie, Darmstadt, 1996.
[37] G. M. Sheldrick, 'SADABS', University of Göttingen, 1997.
[38] E. M. McCarron III, D. M. Thomas, J. C. Calabrese, *Inorg. Chem.* **1987**, *26*, 370.
[39] J. Guo, P. Zavalij, M. S. Whittingham, *J. Solid State Chem.* **1995**, *117*, 323.
[40] J.-M. Reau, C. Fouassier, P. Hagenmuller, *Bull. Soc. Chim. Fr.* **1971**, *8*, 2883.
[41] K. Eda, K. Chin, M. S. Whittingham, *Chem. Lett.* **1999**, 811.
[42] N. E. Breese, M. O'Keefe, *Acta Crystallogr.*, *Sect. B* **1991**, *47*, 192.
[43] R. D. Shannon, C. T. Prewitt, *Acta Crystallogr.*, *Sect. B* **1969**, *25*, 925.
[44] B. M. Gatehouse, B. K. Miskin, *J. Solid State Chem.* **1975**, *15*, 274.
[45] B. M. Gatehouse, B. K. Miskin, *J. Solid State Chem.* **1974**, *9*, 247.
[46] K. A. Wilhelmi, K. Waltersson, L. Kihlborg, *Acta Chem. Scand.* **1971**, *25*, 2675.
[47] H. Richter, J. Fuchs, *Z. Naturforsch.*, *B* **1984**, *39*, 623.
[48] R. Benchrifa, M. Leblanc, R. De Pape, *Eur. J. Solid State Inorg. Chem.* **1989**, *26*, 593.
[49] A. Briceño, R. Atencio, *Acta Crystallogr.*, *Sect. E* **2004**, *60*, i47.
[50] K. Eda, K. Chin, N. Sotani, M. S. Whittingham, *J. Solid State Chem.* **2004**, *177*, 916.
[51] P. Caillet, *Bull. Soc. Chim. Fr.* **1967**, *12*, 4750.
[52] J.-M. Reau, C. Fouassier, *Bull. Soc. Chim. Fr.* **1971**, *2*, 398.
[53] J. Marrot, J.-M. Savariault, *Acta Crystallogr.*, *Sect. C* **1995**, *51*, 2201.
[54] N. L. Misra, K. L. Chawla, V. Venugopal, D. D. Sood, *J. Alloys Comp.* **1999**, *284*, 112.
[55] W. Lasocha, A. Rafalska-Lasocha, H. Schenk, *Cryst. Res. Technol.* **1997**, *32*, 577.
[56] W. Lasocha, J. Jansen, H. Schenk, *J. Solid State Chem.* **1995**, *115*, 225.
[57] H.-U. Kreusler, A. Förster, J. Fuchs, *Z. Naturforsch.*, *B* **1980**, *35*, 242.
[58] S. Hodorowicz, E. Hodorowicz, S. Sagnowski, W. Surga, *Pol. J. Chem.* **1980**, *54*, 1859.
[59] K. Sjöbom, B. Hedman, *Acta Chem. Scand.* **1973**, *27*, 3673.
[60] H. T. Evans, B. M. Gatehouse, P. Leverett, *J. Chem. Soc.*, *Dalton Trans.* **1975**, *6*, 505.
[61] U. Kortz, M. T. Pope, *Acta Crystallogr.*, *Sect. C* **1995**, *51*, 1717.
[62] B. Kamenar, B. Kaitner, N. Strukan, *Acta Crystallogr.*, *Sect. C* **1990**, *46*, 2249.
[63] A. J. Bridgeman, *J. Phys. Chem. A* **2002**, *106*, 12151.
[64] R. Mattes, K. Mennemann, N. Jäckel, H. Rieskamp, H.-J. Brockmeyer, *J. Less-Common Metals* **1980**, *76*, 199.
[65] R. Mattes, G. Müller, H. J. Becher, *Z. Anorg. Allg. Chem.* **1972**, *389*, 177.

[66] V. S. Sergienko, M. A. Porai-Koshits, T. S. Khodashova, *Zh. Strukt. Khim.* **1972**, *3*, 461.
[67] D. Grandjean, R. Weiss, *Bull. Soc. Chim. Fr.* **1967**, *8*, 3040.
[68] G. Pausewang, W. Rüdorff, *Z. Anorg. Allg. Chem.* **1969**, *364*, 69.
[69] A. Michailovski, M. Wörle, G. R. Patzke, in preparation.
[70] M. L. Niven, J. J. Cruywagen, J. B. B. Heyns, *J. Chem. Soc.*, *Dalton Trans.* **1991**, 2007.
[71] I. Böschen, B. Buss, B. Krebs, *Acta Crystallogr.*, *Sect. B* **1974**, *30*, 48.
[72] M. Isobe, F. Marumo, T. Yamase, T. Ikawa, *Acta Crystallogr.*, *Sect. B* **1978**, *34*, 2728.
[73] E. M. McCarron III, J. F. Whitney, D. B. Chase, *Inorg. Chem.* **1984**, *21*, 3275.
[74] B. Kamenar, M. Penavic, B. Markovic, *Acta Crystallogr.*, *Sect. C* **1988**, *44*, 1521.
[75] X. You, J. Chen, Z. Xu, J. Huang, *Acta Crystallogr.*, *Sect. C* **1989**, *45*, 413.
[76] P. V. Klevtsov, L. A. Glinskaya, R. F. Klevtsova, K. S. Aleksandrov, *J. Struct. Chem.* **1997**, *38*, 615.
[77] A. Michailovski, G. R. Patzke, to be published.
[78] J.-D. Grunwaldt, M. Ramin, M. Rohr, A. Michailovski, G. R. Patzke, A. Baiker, *Rev. Sci. Instr.* **2005**, *76*, 054104.
[79] A. Michailovski, J.-D. Grunwaldt, A. Baiker, R. Kiebach, W. Bensch, G. R. Patzke, *Angew. Chem.*, submitted.
[80] W. Surga, *Pol. J. Chem.* **1987**, *61*, 33.

Received April 12, 2005